Center for Turbulence Research
Proceedings of the Summer Program 2008

An adaptive local deconvolution model for compressible turbulence

By S. Hickel† AND J. Larsson

The objective of this project was the analysis and the control of local truncation errors in large eddy simulations. We show that physical reasoning can be incorporated into the design of discretization schemes. Using systematic procedures, a non-linear discretization method is developed where numerical and turbulence-theoretical modeling are fully merged. The truncation error itself functions as an implicit turbulence model which accurately represents the effects of unresolved turbulence.

1. Introduction

Turbulence modeling and the numerical discretization of the Navier-Stokes equations are strongly coupled in large eddy simulations (LES). Since subgrid-scale (SGS) models generally operate on scales that are only marginally resolved by the underlying numerical method, the truncation error of common approximations for the convective terms can outweigh the effect of even physically sound models. This mutual interference can have large and generally unpredictable effects on the accuracy of the solution. A different approach is to exploit this link by developing discretization methods from subgrid-scale models, or vice versa. Approaches where SGS models and numerical discretizations are fully merged are called implicit LES (ILES).

SGS effects are modeled *explicitly* if the underlying conservation law is modified and subsequently discretized. The filtering concept of Leonard (1974) is commonly employed for deriving explicit SGS models without reference to a computational grid and without taking into account a discretization scheme. As implicit modeling we denote the situation when the unmodified conservation law is discretized and the numerical truncation error acts as an SGS model. Since this SGS model is *implicitly* contained within the discretization scheme, an explicit computation of model terms becomes unnecessary.

Most previous approaches to implicit SGS modeling have relied on the application of pre-existing discretization schemes to fluid-flow turbulence. Consequently, methods with suitable implicit SGS models have usually been found by trial and error, which has led to the common belief that an implicit subgrid-scale model is merely inferred by the choice of discretization. Comparative studies have shown that stabilizing under-resolved simulations by upwind or non-oscillatory schemes is insufficient for accurately representing SGS turbulence. For example, Honein & Moin (2005) found that traditional ILES required differently tuned parameters to predict the correct decay rates of different quantities. Employing implicit LES for prediction requires numerical methods that are specially designed, optimized and validated for the particular differential equation to be solved. A full coupling of the SGS model and the discretization scheme cannot be achieved without incorporating physical reasoning into the design of the implicit SGS model.

† Technische Universität München, Germany

Implicit SGS modeling requires procedures for design, analysis and optimization of non-linear discretization schemes. In order to improve on the aforementioned modeling uncertainties, we have proposed a systematic framework for implicit LES. The resulting adaptive local deconvolution method (ALDM) for implicit LES is based on a non-linear deconvolution operator and a numerical flux function (Adams *et al.* 2004; Hickel *et al.* 2006). Free parameters inherent to the discretization allow for the truncation error to be calibrated such that it acts as a physically motivated SGS model. ALDM has shown the potential for providing a reliable, accurate and efficient method for LES. Various applications, such as 3-D homogeneous isotropic turbulence, transitional and turbulent plane channel flow and turbulent boundary-layer separation, have demonstrated the good performance of the implicit model. Computational results agree well with theory and experimental data, and show that a carefully designed implicit SGS model can perform at least as well as established explicit models; in fact, for most considered applications the performance is actually better. This is possible because physical reasoning is incorporated into the design of the discretization scheme and discretization effects are fully taken into account within the SGS model formulation.

The method is established for LES of turbulent flows governed by the incompressible Navier-Stokes equations and for passive-scalar mixing (Hickel & Adams 2007; Hickel *et al.* 2007). The subject of this paper is the extension of the methodology to ILES of compressible turbulence.

2. Discretization design

2.1. *The ALDM approach*

For brevity of notation, the following summary of the basic ideas behind ALDM is given for a 1-D case and a generic non-linear transport equation

$$\partial_t u + \partial_x F(u) = 0 \ . \tag{2.1}$$

Following Leonard (1974) the discretized equation is obtained by convolution with a homogeneous filter kernel G and the subsequent discretization

$$\partial_t \overline{u}_N + G * \partial_x F_N(u_N) = -G * \partial_x \tau_{SGS} \ , \tag{2.2}$$

where the overbar denotes the filtering

$$\overline{u}(x) = \int_{-\infty}^{+\infty} G(x - x')u(x')dx' = G * u \ , \tag{2.3}$$

and the subscript N indicates grid functions obtained by projecting continuous functions onto the numerical grid $x_N = \{x_j\}$. The subgrid-stress tensor

$$\tau_{SGS} = F(u) - F_N(u_N) \tag{2.4}$$

originates from the grid projection of non-linear terms and has to be modeled in order to close Eq. (2.2). With Leonard's approach the filtering of the continuous system is considered as predominant approximation where the numerical error in solving this continuous system is supposed to be negligibly small. Consequently, explicit SGS models are usually derived without reference to a computational grid and without taking into account any discretization scheme.

The unfiltered, i.e., continuous, solution u is unknown in LES. However, accurate approximations $\widetilde{u}_N$ of the discrete grid function u_N can be obtained from $\overline{u}_N$ by regularized deconvolution. Hence, the solution $\overline{u}_N$ obtained with the discrete operators does not satisfy Eq. (2.2), but rather a modified differential equation

$$\partial_t \overline{u}_N + G * \partial_x F_N(u_N) = \mathcal{G}_N - \widetilde{G} * \widetilde{\partial}_x \widetilde{\tau}_{SGS} \ . \tag{2.5}$$

Solved numerically, the discrete approximation of the SGS model interferes with the truncation error of the underlying discretization scheme

$$\mathcal{G}_N = G * \partial_x F_N(u_N) - \widetilde{G} * \widetilde{\partial}_x \widetilde{F}_N(\widetilde{u}_N) \ , \tag{2.6}$$

where a tilde indicates the respective numerical approximation. This interference of model and discretization is exploited in implicit LES. Particularly, an explicit SGS model is resembled if the filtered divergence of the model SGS tensor is approximated by

$$\mathcal{G}_N \approx -G * \partial_x \tau_{SGS} \tag{2.7}$$

so that no model terms have to be computed explicitly during time advancement. With ALDM numerical discretization and SGS modeling are merged entirely. The discrete system for evolving a grid-function approximation is considered directly as a truncated representation of the unmodified continuous system (2.1).

A suitable environment for the discretization design is provided by Schumann's concept of a finite-volume method (Schumann 1975). The averaging and reconstruction steps that are involved in finite-volume discretizations are related to the filtering and deconvolution that are well known in explicit SGS modeling. An advantageous aspect is the fact that the numerical truncation error of finite-volume methods readily appears as a divergence of a tensor, as required for physically motivated implicit modeling by Eq. (2.7).

Although filtering is not performed explicitly, we can use the filter formulation of Leonard as an analytical tool when designing and analyzing the discrete operators. A finite-volume discretization corresponds to the evaluation of Eq. (2.2) with a top-hat filter

$$G(x - x_j, h) = \begin{cases} 1/h & , \ |x - x_j| \le h/2 \\ 0 & , \ \text{else} \end{cases} \ , \tag{2.8}$$

on a computational grid with spacing h. With ALDM, a local reconstruction of the unfiltered solution is obtained from a solution-adaptive combination

$$\widetilde{u}^{\mp}(x_{j\pm1/2}) = \sum_{k=1}^{K} \sum_{r=0}^{k-1} \omega_{k,r}^{\mp}(\gamma_{k,r}, \overline{u}_N) \widetilde{p}_{k,r}^{\mp}(x_{j\pm1/2}) \tag{2.9}$$

of Harten-type deconvolution polynomials

$$\widetilde{p}_{k,r}^{\mp}(x_{j\pm1/2}) = \sum_{l=0}^{k-1} c_{k,r,l}^{\mp}(x_N) \overline{u}_{j-r+l} \ , \tag{2.10}$$

where half-integer indices denote reconstructions at the cell faces. The grid-dependent coefficients $c_{k,r,l}^{\mp}$ are chosen such that

$$\widetilde{p}_{k,r}^{\mp}(x_{j\pm1/2}) = u(x_{j\pm1/2}) + \mathcal{O}\left(h^k\right) \ . \tag{2.11}$$

Adaptivity of the deconvolution operator is achieved by dynamically weighing the respective contributions by $\omega_{k,r}(\gamma_{k,r}, \overline{u}_N)$, where $\gamma_{k,r}$ are free model parameters. Instead of maximizing the order of accuracy, deconvolution is regularized by limiting the degree

k of local approximation polynomials to $k \leq K$ and by permitting all polynomials of degree $1 \leq k \leq K = 3$ to contribute to the approximately deconvolved solution. Secondary regularization is provided by a suitable consistent numerical flux function

$$\widetilde{F}_N(x_{j\pm1/2}) = F\left(\frac{1}{2}\left(\widetilde{u}^-_{j\pm1/2} + \widetilde{u}^+_{j\pm1/2}\right)\right) - R(\sigma, \overline{u}, \widetilde{u})\left(\widetilde{u}^+_{j\pm1/2} - \widetilde{u}^-_{j\pm1/2}\right) \ , \tag{2.12}$$

where R can be any non-negative, shift-invariant functional of $\overline{u}$ and $\widetilde{u}$ which needs to defined specifically for the particular differential equation.

The solution-adaptive stencil-selection scheme and the numerical flux function contain free parameters $\{\gamma_{k,r}, \sigma\}$ which can be used to adjust the spatial truncation error of the discretization. For implicit SGS modeling, the values of these free parameters are determined in such a way that the truncation error $\mathcal{G}_N$ of the discretization method acts as a physically motivated SGS model.

Explicit deconvolution-type SGS models have so far been limited to linear deconvolution. ALDM extends, by employing methods that are well established for essentially non-oscillatory finite-volume discretizations, the concept of approximate deconvolution to the solution-adaptive non-linear case. The resulting method represents a full merging of numerical discretization and SGS model. Incorporating the essential elements of LES, filtering and deconvolution, the implicit model of ALDM combines an implicit tensor-dissipation regularization with a generalized scale-similarity approach.

2.2. *ALDM for compressible turbulence*

We consider the 3-D compressible Navier-Stokes equations in conservative form

$$\partial_t \boldsymbol{U} + \nabla \cdot \boldsymbol{F}(\boldsymbol{U}) + \nabla \cdot \boldsymbol{D}(\boldsymbol{U}) = 0 \tag{2.13}$$

with the solution vector $\boldsymbol{U} = [\rho, \rho u_1, \rho u_2, \rho u_3, E]$. The conserved variables are density ρ, momentum ρu_i and total energy E. For later convenience, the flux is split in the convective part

$$\boldsymbol{F}_i(\boldsymbol{U}) = [\ u_i\rho,\ u_i\rho u_1 + \delta_{i1}p,\ u_i\rho u_2 + \delta_{i2}p,\ u_i\rho u_3 + \delta_{i3}p,\ u_i(E+p)\ ] \tag{2.14}$$

and the viscous part

$$\boldsymbol{D}_i(\boldsymbol{U}) = [\ 0,\ -\tau_{i1},\ -\tau_{i2},\ -\tau_{i3},\ -u_k\tau_{ik} + q_i\ ] \tag{2.15}$$

where u_i is the velocity vector, τ_{ij} denotes the viscous stress tensor

$$\tau_{ij} = \mu(T)(\partial_j u_i + \partial_i u_j - 2/3\delta_{ij}\partial_k u_k) \ , \tag{2.16}$$

and the heat flux in the energy equation is

$$q_i = -\kappa(T)\partial_i T \ . \tag{2.17}$$

The above equations are solved in dimensionless form. By assuming an ideal gas, the governing flow parameters are the Reynolds number Re, the Prandtl number Pr, the Mach number Ma and the ratio of specific heats γ. The pressure p and temperature T are determined by the definition of the total energy

$$E = \frac{1}{\gamma - 1}p + \frac{1}{2}\rho u^2 \tag{2.18}$$

and the ideal-gas equation of state

$$T = \gamma \mathrm{Ma}^2 \frac{p}{\rho} \ . \tag{2.19}$$

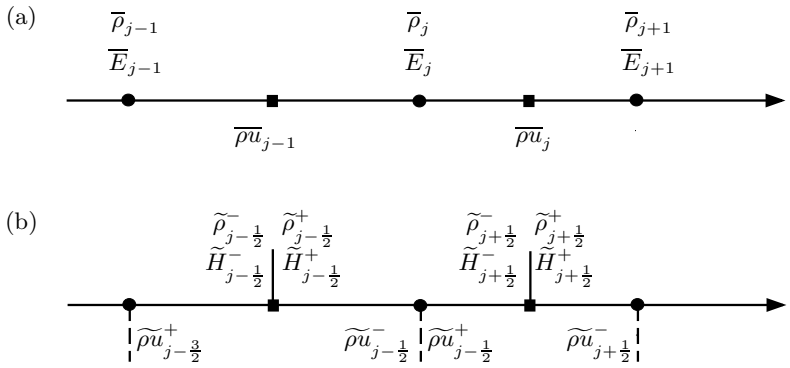

FIGURE 1. Staggered grid arrangement. (a) Filtered solution. (b) Reconstructions of unfiltered solution in a finite-volume discretization.

A power law is assumed for the temperature dependence of viscosity

$$\mu = \frac{T^{0.67}}{\mathrm{Re}} \tag{2.20}$$

and thermal conductivity

$$\kappa = \mu \frac{1}{(\gamma - 1)\mathrm{Ma}^2 \mathrm{Pr}} \ . \tag{2.21}$$

For implicit SGS modeling we essentially focus on the hyperbolic flux $\boldsymbol{F}$, whose discretization causes the SGS effects of interest. The novel discretization is derived for $\nabla \cdot \boldsymbol{F}$, whereas standard centered differences are used for discretizing the viscous flux $\boldsymbol{D}$. The discretization of the viscous flux $\boldsymbol{D}$ has negligible influence on the results of LES at large Reynolds number, since the grid cutoff is typically chosen to be within the inertial range.

The starting point of this work is provided by our established methodology for implicit LES of incompressible turbulence and passive scalar mixing. For this reason, a staggered Cartesian grid is considered in this paper. Density, energy and the thermodynamic quantities are discretized on the primary grid, whereas the control volumes of the momentum are staggered by half a cell (see Fig. 1). An analogous scheme for collocated grids, which appears to be superior when turbulence interacts with shocks, is currently under development and will be published elsewhere.

The numerical building blocks of finite-volume methods are a reconstruction of the unfiltered solution at cell faces, a numerical flux function that works on the reconstructed solution, and a numerical integration scheme to compute the face-averaged flux.

The local adaptive reconstruction scheme of ALDM has been outlined above. Here, it is applied to density, velocity, momentum and enthalpy $H = E + p$. The computational costs of a multi-dimensional finite-volume scheme strongly depends on the implementation of the reconstruction step. An efficient method for the 3-D reconstruction scheme of ALDM is given in Hickel & Adams (2006). This simplified adaptive local deconvolution (SALD) method reduces the amount of computational operations without affecting the quality of the LES results. The SALD implementation is used for all computations in this paper.

During computational experimentation it became apparent that the formulation of the transporting velocities for density and enthalpy is crucial. Several seemingly consistent

definitions, such as the form proposed by Hickel *et al.* (2007) for passive-scalar mixing, led to a strong over-estimation of the dilatational velocity, though all other monitored quantities were accurately predicted. We finally found that

$$\begin{aligned}
\widetilde{u}^o_{ijk} &= 2\overline{\rho u}_{ijk} \;/\; (\widetilde{\rho}^+_{i+\frac{1}{2}\;jk} + \widetilde{\rho}^-_{i+\frac{1}{2}\;jk}) \\
\widetilde{v}^o_{ijk} &= 2\overline{\rho v}_{ijk} \;/\; (\widetilde{\rho}^+_{ij+\frac{1}{2}\;k} + \widetilde{\rho}^-_{ij+\frac{1}{2}\;k}) \\
\widetilde{w}^o_{ijk} &= 2\overline{\rho w}_{ijk} \;/\; (\widetilde{\rho}^+_{ijk+\frac{1}{2}} + \widetilde{\rho}^-_{ijk+\frac{1}{2}})
\end{aligned} \tag{2.22}$$

results in a proper scaling of the dilatation. Note that we use $\{u, v, w\}$ and $\{\rho u, \rho v, \rho w\}$ synonymously with $\{u_1, u_2, u_3\}$ and $\{\rho u_1, \rho u_2, \rho u_3\}$ in the following.

With these prerequisites, the numerical flux function $\widetilde{\boldsymbol{F}}$ can be defined. The proposed numerical flux consists of two parts. The first term corresponds to the physical Navier-Stokes flux. For maximum order of consistency it is computed from the mean of both reconstructions of the unfiltered solution at the considered cell face. Note that this modification of the Lax-Friedrichs approach (where the flux is averaged) results in a skew-symmetric like discretization with favorable aliasing behavior. The difference between both interpolants is exploited in a second term as an estimate of the local truncation error. The numerical flux for the continuity equation and the energy equation is

$$\begin{aligned}
\widetilde{F}_\phi = \frac{1}{2} &\begin{bmatrix} \widetilde{u}^o_{i-1\;jk}\;(\widetilde{\phi}^+_{i-\frac{1}{2}\;jk} + \widetilde{\phi}^-_{i-\frac{1}{2}\;jk}) \\ \widetilde{v}^o_{ij-1\;k}\;(\widetilde{\phi}^+_{ij-\frac{1}{2}\;k} + \widetilde{\phi}^-_{ij-\frac{1}{2}\;k}) \\ \widetilde{w}^o_{ijk-1}\;(\widetilde{\phi}^+_{ijk-\frac{1}{2}} + \widetilde{\phi}^-_{ijk-\frac{1}{2}}) \end{bmatrix} \\
- \sigma_\phi &\begin{bmatrix} |\widetilde{u}^+_{i-\frac{3}{2}\;jk} - \widetilde{u}^-_{i-\frac{1}{2}\;jk}|\;(\widetilde{\phi}^+_{i-\frac{1}{2}\;jk} - \widetilde{\phi}^-_{i-\frac{1}{2}\;jk}) \\ |\widetilde{v}^+_{ij-\frac{3}{2}\;k} - \widetilde{v}^-_{ij-\frac{1}{2}\;k}|\;(\widetilde{\phi}^+_{ij-\frac{1}{2}\;k} - \widetilde{\phi}^-_{ij-\frac{1}{2}\;k}) \\ |\widetilde{w}^+_{ijk-\frac{3}{2}} - \widetilde{w}^-_{ijk-\frac{1}{2}}|\;(\widetilde{\phi}^+_{ijk-\frac{1}{2}} - \widetilde{\phi}^-_{ijk-\frac{1}{2}}) \end{bmatrix},
\end{aligned} \tag{2.23}$$

where ϕ has to be replaced by ρ and H, respectively. The numerical flux for the first momentum equation is

$$\begin{aligned}
\widetilde{F}_{\rho u} = \frac{1}{4} &\begin{bmatrix} (\widetilde{u}^+_{i-\frac{1}{2}\;j\;k} + \widetilde{u}^-_{i-\frac{1}{2}\;j\;k})\;(\widetilde{\rho u}^+_{i-\frac{1}{2}\;jk} + \widetilde{\rho u}^-_{i-\frac{1}{2}\;jk}) + p_{ijk} \\ (\widetilde{v}^+_{i+\frac{1}{2}\;j-1\;k} + \widetilde{v}^-_{i+\frac{1}{2}\;j-1\;k})\;(\widetilde{\rho u}^+_{ij-\frac{1}{2}\;k} + \widetilde{\rho u}^-_{ij-\frac{1}{2}\;k}) \\ (\widetilde{w}^+_{i+\frac{1}{2}\;j\;k-1} + \widetilde{w}^-_{i+\frac{1}{2}\;j\;k-1})\;(\widetilde{\rho u}^+_{ijk-\frac{1}{2}} + \widetilde{\rho u}^-_{ijk-\frac{1}{2}}) \end{bmatrix} \\
- &\begin{bmatrix} \sigma^*_{\rho u}|\widetilde{u}^+_{i-\frac{1}{2}\;j\;k} - \widetilde{u}^-_{i-\frac{1}{2}\;j\;k}|\;(\widetilde{\rho u}^+_{i-\frac{1}{2}\;jk} - \widetilde{\rho u}^-_{i-\frac{1}{2}\;jk}) \\ \sigma_{\rho u}|\widetilde{v}^+_{i+\frac{1}{2}\;j-1\;k} - \widetilde{v}^-_{i+\frac{1}{2}\;j-1\;k}|\;(\widetilde{\rho u}^+_{ij-\frac{1}{2}\;k} - \widetilde{\rho u}^-_{ij-\frac{1}{2}\;k}) \\ \sigma_{\rho u}|\widetilde{w}^+_{i+\frac{1}{2}\;j\;k-1} - \widetilde{w}^-_{i+\frac{1}{2}\;j\;k-1}|\;(\widetilde{\rho u}^+_{ijk-\frac{1}{2}} - \widetilde{\rho u}^-_{ijk-\frac{1}{2}}) \end{bmatrix},
\end{aligned} \tag{2.24}$$

with the other components of the momentum flux defined analogously. Note that we use different parameters, $\sigma^*_{\rho u}$ versus $\sigma_{\rho u}$, for the diagonal and off-diagonal components of the momentum flux. In total, the numerical flux functions introduce four free parameters $\{\sigma_\rho, \sigma^*_{\rho u}, \sigma_{\rho u}, \sigma_E\}$ that will be used for implicit SGS modeling.

3. Subgrid-scale modeling

3.1. *Analysis*

In classical numerical analysis, truncation errors are analyzed in the limit of small grid size compared to the smallest flow scale, and discretization coefficients are chosen in such a way that the formal order of accuracy of the discretization is maximum. In LES the chosen grid size essentially defines the smallest represented physical scale. In particular for implicit LES, numerical discretization and turbulence model are indistinguishable. Unlike with high-order shock-capturing schemes, such as the WENO method where one tries to maximize the formal order of accuracy for smooth solutions, the free parameters of ALDM are selected in such a way that the truncation error of the discretization acts as a physically motivated SGS model. For the purpose of finding suitable discretization parameters, the modified differential equation of the discretization method is analyzed by measuring the spectral numerical dissipation and diffusion in simulations of freely decaying homogeneous isotropic turbulence. This *a posteriori* analysis follows from the hypothesis that the primary purpose of an SGS model is to provide the correct spectral distribution of the dissipation and diffusion of resolved scales by interactions with modeled SGS stresses. A semi-analytical expression for the eddy viscosity and eddy diffusivity spectrum of isotropic turbulence at high Reynolds numbers was given by Chollet and Lesieur (Chollet 1984) based on the eddy-damped quasi-normal Markovian (EDQNM) theory. Note that this particular form of the eddy viscosity is not enforced. Only for inertial-range isotropic turbulence is it necessarily recovered due to the parameter calibration.

3.2. *Parameter calibration*

For parameter evaluation and optimization we perform LES of isotropic homogeneous turbulence at an infinite computational Reynolds number and Mach number $\mathrm{Ma}_t = 0.3$. The $(2\pi)^3$-periodic computational domain is discretized with 32^3 cells. The initial data is obtained by filtering and truncating data from the inertial range of separate direct numerical simulations (DNS). A set of parameters is evaluated by a cost function, that is defined as the L_2 norm of the deviations of the measured numerical viscosity and diffusivity from a reference based on EDQNM theory. Optimal parameter values that minimize this norm are identified by an automatic optimization algorithm.

In a general scheme, different parameter values for the density, momentum and energy equation are possible, resulting in 16 parameters in total. In order to accelerate the convergence of the optimization algorithm, only the values of the 4 parameters $\{\sigma_\rho, \sigma^*_{\rho u}, \sigma_{\rho u}, \sigma_E\}$ of the flux function are subjected to optimization, whereas the parameters of the reconstruction scheme $\{\gamma_{k,r}\}$ are adopted from the incompressible model without modification.

The cost function is computed from the averaged numerical viscosity and diffusivity spectra from 5 independent simulations, each advanced by 5 time steps. These numbers of time steps and realizations were chosen as a compromise between accuracy and computational feasibility. They are less than what would be necessary to completely remove the effect of stochastic fluctuations. Thus the resulting cost function is not smooth but exhibits residual fluctuations. Unlike standard gradient-approximation based optimization methods, evolutionary algorithms can handle such non-smooth cost functions (Back *et al.* 1997).

Evolutionary optimization algorithms model natural biological processes by simple stochastic search methods. A set of free parameters is considered as the genome of a

Parameter	Value
Number of genes per individual	4
Initialization	Random numbers, equally distributed on $(0, 0.5)$
Number of generations	219
Population	32
Offspring per generation	32
Selection of parents	Tournament
Offspring generation	Arithmetic cross-over and mutation
Mutation model	Gaussian normal distribution, zero mean
Initial mutation variance	0.1
Mutation-variance update factor	0.95
Admissible parameter range	$\geq 0.$
Admissible mutation-variance range	$\left[10^{-6}, 10^{+3}\right]$

TABLE 1. Parameters of the evolutionary optimization algorithm.

Parameter	Value
σ_ρ	0.6699
$\sigma_{\rho u}$	0.6302
$\sigma^*_{\rho u}$	0.0638
σ_E	0.8093

TABLE 2. Optimized parameters.

living individual. The algorithm operates on a population of individuals and applies the survival-of-the-fittest principle of the Darwinian theory of evolution. At each generation, a new set of individuals is created by modeled natural processes, such as selection according to the level of fitness, recombination and random mutation. This process leads to the evolution of a population of individuals that is better adapted to a cost function than the population that it was created from. Since this algorithm works on populations instead of single individuals, the search is performed in an efficient parallel manner. For further details, the reader is referred to Back *et al.* (1997) and the references therein.

The performance and convergence of the employed optimization algorithm strongly depend on the mutation model. We employ normally distributed random numbers. The variance is initially set to $\sigma^2_{\text{mut}} = 0.1$ and updated by a factor of $0.95^{\pm 1}$ after every generation, where successful mutations enlarge the target area and unsuccessful mutations make it smaller. For further details on the algorithm, see Table 1.

Normally distributed random numbers were used as the initial guess for the first population. The subsequent generations are created by a four-step algorithm consisting of parent selection, recombination, mutation and new-population selection. This scheme is iterated until a maximum number of generations is reached. The final set of parameters, which was selected after evaluating 219 generations, each with 32 individuals, is given in Table 2.

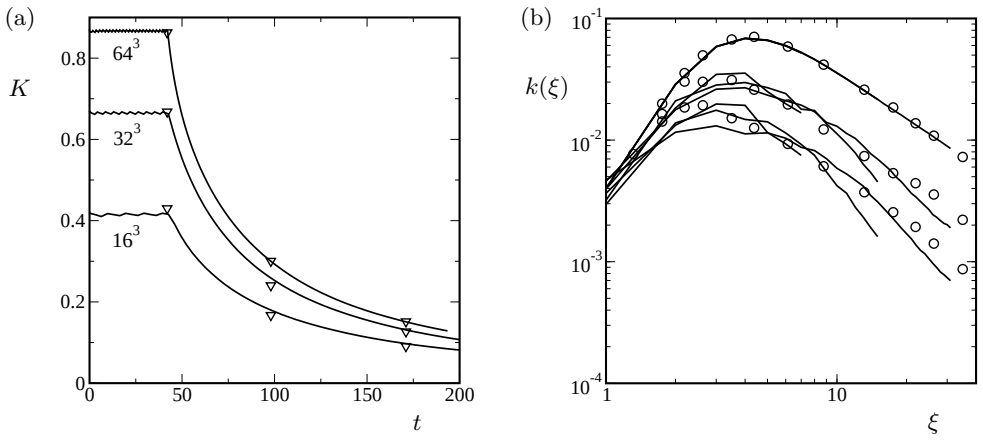

FIGURE 2. Kinetic energy (a) and 3-D kinetic-energy spectra (b) for implicit LES of decaying grid-generated turbulence according to the wind-tunnel experiments of Comte-Bellot & Corrsin (1971). ——— LES results for grid resolutions 16^3, 32^3 and 64^3; $\bigtriangledown$ filtered experimental data; $\bigcirc$ experimental 3-D spectra at three subsequent stations ($t = 42$, $t = 98$, $t = 172$).

4. Validation

4.1. *Comte-Bellot–Corrsin experiment*

The first test case is decaying grid-generated turbulence according to the wind-tunnel experiments of Comte-Bellot & Corrsin (1971), denoted hereafter as CBC. CBC provides streamwise energy spectra for grid-generated turbulence at three positions downstream of a mesh with width $M = 5.08$ cm. Table 3 of CBC gives corresponding 3-D energy spectra which were obtained under the assumption of isotropy. The grid Reynolds number of the experiment is $Re_M = 34,000$, the Taylor-microscale Reynolds number is given as $\mathrm{Re}_\lambda = 71.6$ at the first and $\mathrm{Re}_\lambda = 60.6$ at the last position.

In the simulation this flow is modeled as decaying turbulence in a $(2\pi)^3$-periodic computational domain. Based on the Taylor hypothesis the temporal evolution in the simulation corresponds to a downstream evolution in the wind-tunnel experiment with the experimental mean-flow speed which is approximately constant. The Reynolds number is adapted to the wind-tunnel experiment, while the turbulent Mach number is set to $\mathrm{Ma}_t = 0.1$. Computations are initialized at time $t = 0$ with a random velocity field with a prescribed kinetic energy spectrum to match the first measurement station of CBC. The method of Ristorcelli & Blaisdell (1997) is used to impose consistent initial data for density, velocity dilatation, and total energy. The 3-D kinetic energy spectrum is maintained constant for $0 \leq t \leq 42$ by applying a spectral forcing to the solenoidal velocity field. During this initial transient the random-phase initial solution develops physical flow structures and correlations. This forcing is suspended when the first measuring station of CBC is reached at $t = 42$.

Since the kinetic energy distribution of the initial velocity field is matched to the first measured 3-D energy spectrum, the SGS model is validated by comparing computational and experimental mean values and 3-D spectra of the kinetic energy at later time instants $t = 98$ and $t = 172$ which correspond to the other two measuring stations. Figure 2 shows results for LES at three grids with 16^3, 32^3 and 64^3 cells. The mean kinetic energy agrees very well with the experimental data that has been filtered to the respective grid reso-

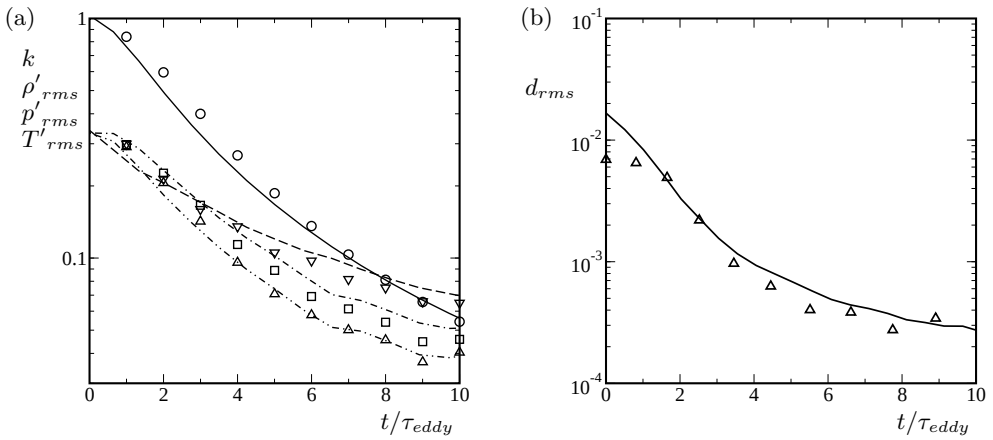

FIGURE 3. Decay of (a) ——— ◯ kinetic energy, —·— □ density, —··— △ pressure, - - - - ▽ temperature, and (b) ——— △ dilatation fluctuations for implicit LES (lines) and filtered DNS (symbols) of compressible isotropic turbulence. The time is given in eddy-turnover times.

lution. Reasonable predictions are obtained for the 3-D spectra (Fig. 2b). These results prove the applicability of the proposed modeling concept to flows in the incompressible limit.

4.2. *Decaying compressible turbulence at $Ma_t = 0.3$*

For a second test we consider decaying turbulence with significant compressibility effects. The initial turbulent Mach number and Taylor-scale Reynolds number are $\mathrm{Ma}_t = 0.3$ and $\mathrm{Re}_\lambda = 100$. The flow is initialized with a random velocity field and prescribed kinetic energy spectrum

$$k(\xi) \sim \xi^4 (exp)(-2\xi^2/\xi_0^2) \ , \tag{4.1}$$

with $\xi_0 = 4$. Consistent initial data for density, velocity dilatation and total energy are imposed as proposed by Ristorcelli & Blaisdell (1997). Contrary to the previous test case, no initial forcing is applied. The decay of the random field starts immediately and may be influenced by the unphysical phases.

The chosen Reynolds number allowed for a DNS at a grid resolution of 128^3 cells that serves as a reference for the implicit LES at a grid resolution of 32^3 cells. Figure 3 shows the time evolutions of the kinetic energy and the fluctuations of density, pressure, temperature and dilatation. Instantaneous spectra at 10 instants in time are shown for kinetic energy, density, pressure and temperature in Fig. 4. The LES results for all quantities compare well with DNS data that has been filtered to the LES resolution. Note that the DNS and LES are different realizations with different random initial data. The model predicts the correct time development of the r.m.s. temperature, density and pressure fluctuations, as well as the proper inertial-range scaling in the spectra.

5. Discussion

The adaptive local deconvolution method (ALDM) was originally developed for incompressible flows, and later extended to include the mixing of a passive scalar. The

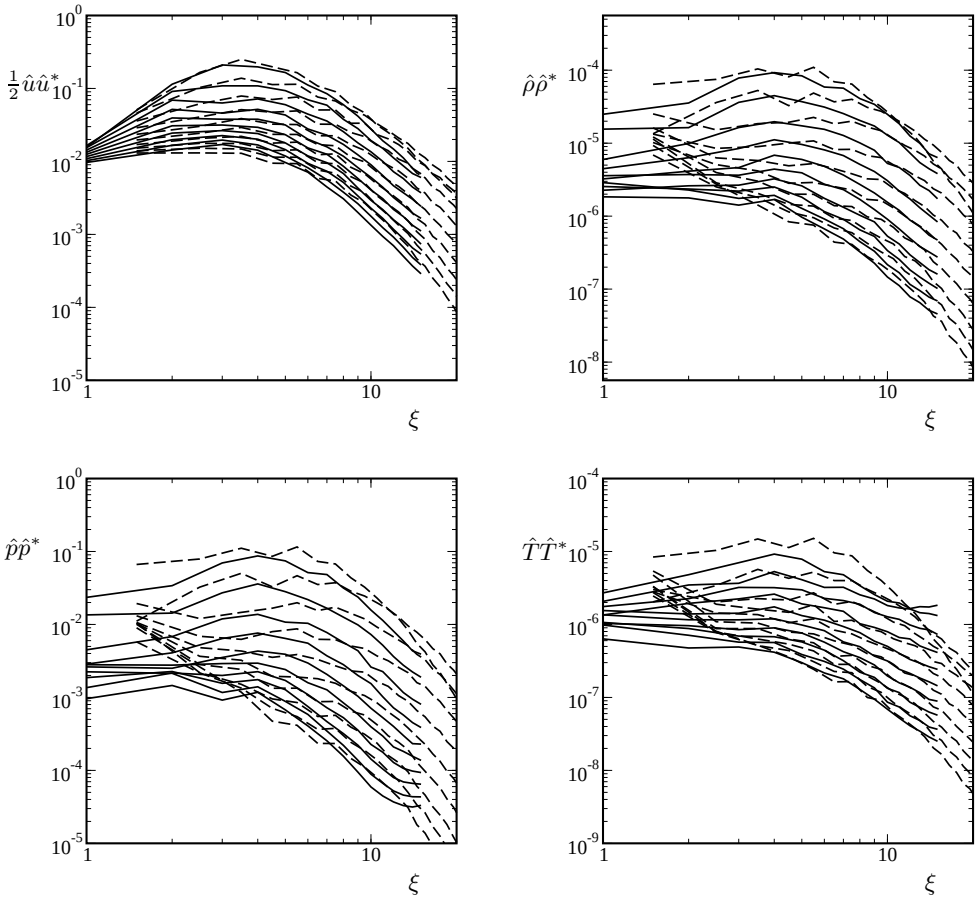

FIGURE 4. 3-D spectra of kinetic energy and variations of density, pressure, temperature for implicit LES of compressible isotropic turbulence. —— LES - - - - DNS.

objective during the 2008 Summer Program was to further extend the method to compressible turbulence.

In incompressible LES only the decay rate of kinetic energy must be predicted; in compressible LES one must also predict the decay rates of the density, pressure, temperature and dilatation fluctuations. In the sense of Kovasznay (1953), compressible LES must correctly model vorticity, entropy and acoustic modes, while the first mode alone is sufficient in incompressible LES. Thus it is not surprising that Honein & Moin (2005) found that traditional implicit LES cannot simultaneously predict the correct decay rates of these different quantities – while it could be tuned for any one quantity (e.g., density fluctuations), this inevitably caused errors in other quantities. This shows that the application of implicit LES to compressible turbulence is non-trivial, and it is in this context that the present work should be viewed.

ALDM was extended to compressible turbulence during the Summer Program, and was implemented in a staggered-grid finite-volume code. A preliminary optimization of the free parameters was done using DNS data of the inertial subrange in isotropic turbulence. The method was then tested by computing two different cases of decaying isotropic

turbulence, at different Mach and Reynolds numbers. The predicted spectra and decay rates of all quantities were found to agree well with experimental data and DNS results, respectively. This is a very encouraging result, especially given the disappointing results in Honein & Moin (2005). We must emphasize that the present results essentially are of a "proof-of-concept" nature: Since the method was optimized on isotropic turbulence, the real test will be a different flow problem. We note that the incompressible ALDM has shown excellent results on several physically complex and canonical flows (despite being optimized for isotropic turbulence). Hence the natural next step is to assess the present method on compressible channel flow. This will be done in future work.

Finally, we note that the flux formulations at the core of the present method should allow for the capturing of shock waves, albeit possibly with different values of the free parameters. Preliminary tests during the Summer Program confirm that this is possible. Thus a second item in future work is to properly investigate how to make the method shock-capturing without sacrificing the excellent turbulence predictions found here.

REFERENCES

Adams, N. A., Hickel, S. & Franz, S. 2004 Implicit subgrid-scale modeling by adaptive deconvolution. *J. Comp. Phys.* **200**, 412–431.

Back, T., Fogel, D. & Michalewicz, Z. 1997 *Handbook of Evolutionary Computation*. Oxford University Press.

Chollet, J.-P. 1984 Two-point closures as a subgrid-scale modeling tool for large-eddy simulations. In *Turbulent Shear Flows IV* (ed. F. Durst & B. Launder), pp. 62–72. Heidelberg: Springer.

Comte-Bellot, G. & Corrsin, S. 1971 Simple Eulerian time correlation of full and narrow-band velocity signals in grid-generated 'isotropic' turbulence. *J. Fluid Mech.* **48**, 273–337.

Hickel, S. & Adams, N. A. 2006 Efficient implementation of nonlinear deconvolution methods for implicit large-eddy simulation. In *High Performance Computing in Science and Engineering. Transactions of the High Performance Computing Center, Stuttgart (HLRS)* (ed. W. Nagel, W. Jäger & M. Resch), pp. 293–306. Springer.

Hickel, S. & Adams, N. A. 2007 On implicit subgrid-scale modeling in wall-bounded flows. *Phys. Fluids* **19**, 105106.

Hickel, S., Adams, N. A. & Domaradzki, J. A. 2006 An adaptive local deconvolution method for implicit LES. *J. Comp. Phys.* **213**, 413–436.

Hickel, S., Adams, N. A. & Mansour, N. N. 2007 Implicit subgrid-scale modeling for large-eddy simulation of passive-scalar mixing. *Phys. Fluids* **19**, 095102.

Honein, A. E. & Moin, P. 2005 Numerical aspects of compressible turbulence simulations. Report TF-92. Department of Mechanical Engineering, Stanford University.

Kovasznay, L. S. G. 1953 Turbulence in supersonic flow. *J. Aero. Sci.* **20** (10), 657–674, Reprinted in *AIAA J.* **41** (7), 2003.

Leonard, A. 1974 Energy cascade in large eddy simulations of turbulent fluid flows. *Adv. Geophys.* **18A**, 237–248.

Ristorcelli, J. R. & Blaisdell, G. A. 1997 Consistent initial conditions for the dns of compressible turbulence. *Physics of Fluids* **9** (1), 4–6.

Schumann, U. 1975 Subgrid scale model for finite-difference simulations of turbulence in plane channels and annuli. *J. Comp. Phys.* **18**, 376–404.